ACS Photonics

Article

pubs.acs.org/journal/apchd5

Extreme Subwavelength Metal Oxide Direct and Complementary Metamaterials

Simon A. Gregory,[†] Yudong Wang,[†,‡] C.H. de Groot,[‡] and Otto L. Muskens*[,†]

[†]Physics and Astronomy, Faculty of Physical Sciences and Engineering, and [‡]Nano Group, Faculty of Physical Sciences and Engineering, University of Southampton, Southampton, SO17 1BJ, United Kingdom

Supporting Information

ABSTRACT: Alternative plasmonic materials like conducting oxides are of great interest for extending the application range of plasmonic and metamaterials with functionalities complementary to traditional noble metals. Here, we investigate the feasibility and limitations of using metal oxides as magnetic resonators for metamaterials and demonstrate that split ring resonators fabricated out of conducting metal oxides show pronounced magnetic and electric modes. The low negative permittivity of the oxide material results in ultrasmall resonant metamolecules, which show only weak interparticle coupling and which consequently allow rational design of extremely dense metamaterials with up to 80 elements per square wavelength and without any significant cross-coupling between elements. Broadband transmission response of up to 50% is obtained over an octave spreading bandwidth using a single-layer design. We numerically explore the tuning of such metal oxide metamaterials through modification of the carrier concentration, offering a prospect which is not available in noble metals. Next to direct designs, we experimentally investigate indium−tin oxide complementary metamaterials obtained using focused ion beam milling. The frequency response of the inverse structures is shown to be complementary to the direct designs following Babinet's principle, while penetration of fields results in an additional loss and lower performance of the complementary structures compared to direct designs. While ITO metamaterials cannot compete with traditional noble metals in their plasmonic performance, the extremely subwavelength scale of metal oxide resonators in combination with favorable properties such as tunability and visible-range transparency may find use in high-spatial frequency and nonlinear metasurfaces.

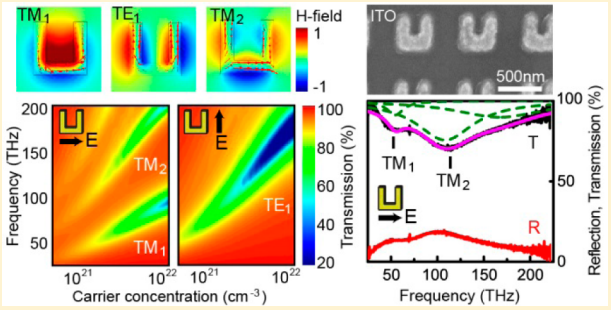

KEYWORDS: *metamaterials, metasurface, plasmonics, split ring resonator, transparent conducting oxides, indium tin oxide*

Metamaterials are subject to much interest due to their improved capabilities compared to natural materials in controlling the flow of light.[1,2] The concept of a metamaterial is one built from man-made, subwavelength components ("metamolecules"), resulting in a material with effective medium characteristics defined by the metamolecule properties and arrangement. Metamaterials research has led to a tremendously active field which has yielded a range of significant discoveries such as negative index of refraction, cloaking, perfect lenses, and tailoring of absorption and blackbody emission.[3−8] Alongside completely new physics, the potential of designing arbitrary phase and polarization properties of radiation using subwavelength resonant nanostructures has enabled enormous freedom in the engineering of new types of photonic components with an extremely small form factor. Metamaterials, and more recently phase discontinuity metasurfaces, are rapidly entering into new domains such as flat optics, holography, spectral filters, and structural coloring.[9−13] It has been increasingly recognized that the combination of metamaterial designs with other functionalities may be able to unlock even more applications. This approach includes combining conventional metamolecules with functional materials,[2,14−16] developing reconfigurable assemblies,[17] or building the metamolecules themselves from new materials,[18] notably in dielectric metasurfaces.[19−22] The search for new materials can be considered as part of a wider activity in plasmonics, which seeks to overcome challenges and limitations in conventional plasmonic materials.[23−32] These include mitigating losses,[33] achieving tunable properties[34,35] and compatibility with silicon technology processes.[36,37]

Transparent conducting oxides form a promising class of materials with the potential to provide new properties in near and mid-IR plasmonics.[38−42] Technologically, oxide materials are of great importance, with many applications in electronics,[43] solar cells,[44,45] photocatalysis,[46] and gas sensors.[47,48] Transparent conducting oxides (TCOs) combine high DC conductivity with high transparency at visible wavelengths. Of these, indium tin oxide (ITO) is perhaps the best known, because of its wide use as a transparent contact in display screens and solar cells. The Drude metal-like properties of the dopant electrons in ITO result in collective oscillations similar

Received: October 14, 2014
Published: April 23, 2015

DOI: 10.1021/acsphotonics.5b00089
ACS Photonics 2015, 2, 606−614

to those found in noble metals but at much longer wavelengths. Furthermore, the dielectric properties of ITO are tunable through the carrier concentration or growth conditions,[23,38] allowing resonance tuning at the fabrication stage. The possibility of dynamic tuning by electrical gating or optical excitation opens up opportunities for nanoscale switching devices.[34,35,49,50] The near-zero permittivity of TCOs in the near-infrared enables completely new types of applications, such as metatronic nanocircuits,[51] epsilon-near-zero response[52] and stopped light.[53] Recently, the first planar TCO metamaterials were demonstrated showing hyperbolic dispersion properties.[54] The performance of TCOs in conventional metamaterial designs is yet an open question.

Here, we experimentally demonstrate split ring resonator (SRR) metamaterials made from ITO with a pronounced resonant optical response in the mid-infrared. The resonant behavior of U-shaped SRR metamaterials is well understood,[55] and the simple design is conducive to fabrication. The metamaterials allow clear assignment of magnetic and electric dipole resonances, which show spectral resonance positions and quality factors in close agreement with numerical predictions. By comparing the ITO metamaterials to identical metamaterial arrays made using Au, the performance of SRRs made from ITO is directly compared. We find that the reduced surface plasmon frequency results in a strong redshift of the ITO response, allowing much more compact metamolecules and high density metamaterials than for an equivalent metamaterial made from Au. While the interaction strength with light of the ITO metamolecules is smaller than for the case of Au, the response of the very high-density metamaterial is greatly simplified by the concomitantly reduced electromagnetic interactions between the metamolecules. This reduced simplicity will be of interest for applications such as phase discontinuity metasurfaces, where precise addressing of the phase response of individual, closely spaced nanoresonators, that is, without cross-coupling, is highly desirable.[9−12] Next to direct metamaterial structures fabricated using e-beam lithography, inverse metamaterial arrays are obtained using focused ion beam milling to demonstrate the complementary properties following Babinet's principle.

RESULTS

Three different U-shaped SRR were fabricated using e-beam lithography followed by evaporation and lift-off. The SRR design dimensions w were 325, 350, and 400 nm, with an arm width of 100 nm and a vertical thickness of 80 nm. For each SRR size, square arrays of 120 × 120 μm^2 area were produced. Figure 1a shows typical Scanning Electron Microscopy images of the three different SRR arrays.

Good quality metamolecule shapes were obtained for the w = 400 nm arrays, while the smaller structures showed a significant reduction of the center gap. Deviations from the design parameters were attributed to e-beam and proximity effects and were obtained similarly for Au arrays in this range of parameters. The quality of the metamolecules directly influences the optical response, as can be seen in Figure 1b,c showing the infrared transmission and reflection for the three different metamolecule sizes for horizontal (TM) and vertical (TE) polarization. Dips are observed in the transmission which corresponds to peaks in reflection at the same frequencies. For the 400 nm wide SRRs, two modes can be clearly distinguished at 50 and 105 THz for TM. As the center gap of the SRRs is reduced for smaller metamolecule sizes, the structure

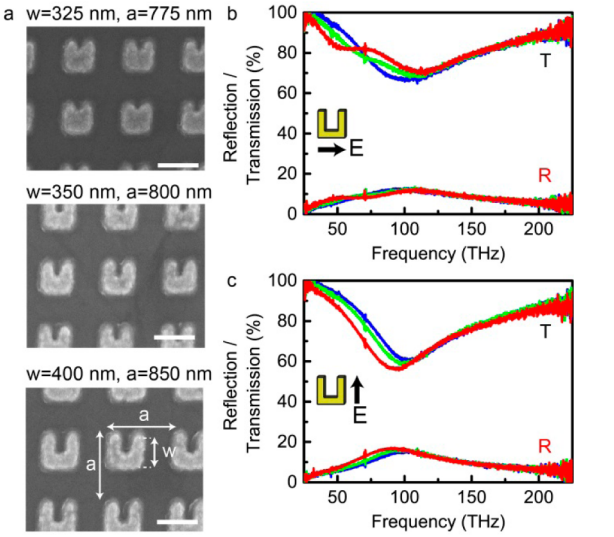

Figure 1. (a) Scanning electron microscopy (SEM) images of ITO arrays of split ring resonators with sizes w = 325, 350, and 400 nm and lattice constant a = 850 nm. Scale bars, 500 nm. Inset: illustration showing definition of parameters w and a. (b, c) Experimental reflection (R) and transmission (T) spectra for ITO metamaterial arrays with w = 325 (blue), 350 (green), and 400 nm (red), for x = 450 nm, for horizontally polarized (b, TM), and vertically polarized (c, TE) incident light.

approaches a square shape and the TM-polarized spectrum in Figure 1b shows only a single resonance identical to the TE-polarization.

Figure 2a,b presents into more detail the spectra for the 400 nm wide SRRs for TM (a) and TE (b) polarizations. The resonances are broad and partially overlapping. Fitting of the FTIR transmission spectra using a superposition of three Lorentzian line profiles was performed to extract the individual resonance parameters. The fits allows us to unambiguously identify three distinct modes in our metamaterial arrays, corresponding to the two lowest order magnetic modes (TM_1, TM_2) and the lowest electric mode (TE_1). The additional higher-frequency Lorentz curves used in the experimental data fitting represent contributions of higher order, broader resonances which we do not consider further in our analysis.

Numerical simulations were performed to complement the experimental results, using the finite element package COMSOL 4.3b. Periodic boundary conditions were used to create infinite arrays of U-shaped SRRs on CaF_2. Scattering boundary conditions were used to provide plane wave excitation and an exit for scattered and transmitted light. These were calculated to obtain relative transmission and reflection, along with loss over the simulation volume.

Using the design parameters of Figure 2a,b (w = 400 nm, a = 850 nm), numerical simulations of ITO metamaterials predict modes at approximately the same frequencies using a carrier concentration of 1.4 × 10^{21} cm^{-3}, close to the value obtained from optical characterization of a plane ITO film fabricated under identical conditions. The presence of resonant modes is associated with enhanced absorption in the ITO, as indicated by the dashed blue lines in Figure 2c,d. Compared to the simulated spectra, the experimental data show some deviations, such as a reduced amplitude of the TM_1 mode compared to the TM_2 magnetic mode, the latter being slightly stronger and broader than in the simulations. The full polarization

DOI: 10.1021/acsphotonics.5b00089
ACS Photonics 2015, 2, 606−614

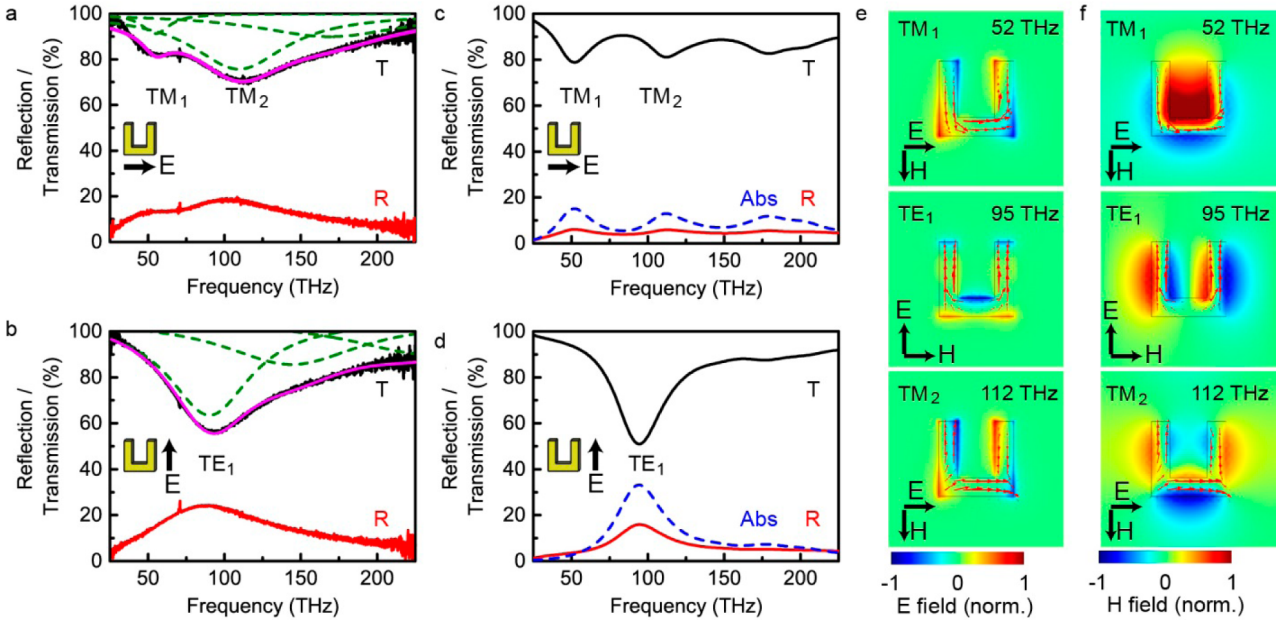

Figure 2. (a, b) Experimental reflection and transmission spectra for w = 400 nm, a = 850 nm ITO metamaterial array for horizontal (a, TM) and vertical (b, TE) polarizations. Experimental transmission spectra have been fitted (purple line) using three Lorentz curves (dashed lines, green) to identify spectral resonances. (c, d) Numerical model simulations of metamaterial array corresponding to experimental data from c and d, blue dashed lines represent absorption. Labels TM_1, TE_1, and TM_2 indicate the first three resonant modes. (e, f) Maps showing out of plane E field (e) and H field (f) for the first three resonant modes, together with vector fields (red arrows), indicating current density.

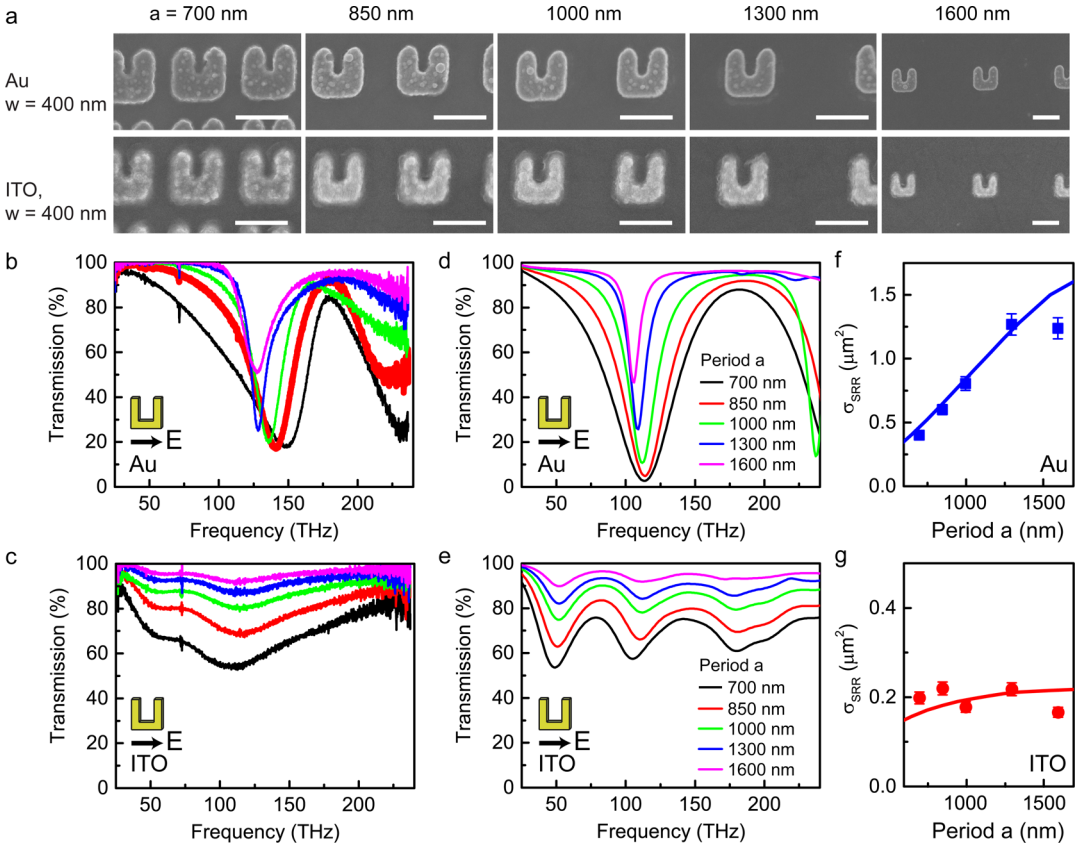

Figure 3. (a) Scanning electron microscopy images of Au and ITO SRRs with sizes of 400 nm and lattice constants a ranging from 700 to 1600 nm. Scale bars, 500 nm. (b, c) Infrared transmission spectra for Au (b) and ITO (c) arrays. (d, e) Simulated transmission spectra for metamaterial arrays with lattice constants corresponding to experimental data. (f, g) Calculated cross section per SRR, σ_{SRR}, for the TM_1 modes of Au (f) and ITO (g). Symbols, experimental data; lines, numerical calculations.

DOI: 10.1021/acsphotonics.5b00089
ACS Photonics 2015, 2, 606−614

dependence of the spectra is presented in Supporting Information, Figure S1, confirming the polarization of the TM and TE modes at 0° and 90°. Some additional broadening is expected from intrinsic variations in shape, carrier density, and possible damping mechanisms in the polycrystalline ITO. Numerical simulations exploring the role of variations in geometry are presented in the Supporting Information, Figures S2 and S3. The effect of these variations is found stronger for the TM than for the TE modes, predicting an additional inhomogeneous broadening of particularly the higher order TM modes. A tentative explanation for the increased strength of the TM_2 compared to the TM_1 mode is offered by the effect of a reduced central gap of the U-shaped SRRs compared to the design (Figure S3), resulting in a partial electric contribution into the TM response.

Overall the model involving realistic Drude parameters provides a reasonable quantitative description of the metamaterial resonance positions without any adjustable parameters. The numerical simulations allow assignment of the magnetic and electric modes. Figure 2e,f shows the out of plane components of the E- and H-fields, respectively, together with vector maps of the current density (arrows), which have been shown to reveal the symmetry of the modes.[55] In particular, the modes are identified by the presence of zero (TM_1), one (TE_1), and two (TM_2) nodes in the current density. The magnetic field component furthermore clearly shows the increasing number of poles over the U-shape.

A detailed comparison between ITO and Au metamaterials of various densities is presented in Figure 3. Previous studies have shown that Au SRR metamaterials show very large electric and magnetic coupling between metamolecules, which results in large modifications of the spectrum.[56] We investigated arrays of 400 nm wide SRRs with lattice constants between 700 and 1600 nm. Figure 3b confirms the large effect of coupling between SRRs for the case of Au metamaterials. For small spacing, the resonance broadens significantly and the transmission amplitude saturates, showing that the extinction cross section per SRR is effectively reduced. In comparison, the extinction for the ITO metamaterial depends much less on lattice constant, and shows an extinction increasing proportional to the surface density as shown in Figure 3c. The experimental trends are reproduced well by numerical simulations, as is shown in Figure 3d,e. From the experimental and simulated spectra, we estimate the extinction cross section per SRR, σ_{SRR}, using the relation $\sigma_{SRR} = (1 - T)a^2$,[56] yielding the results shown in Figure 3f,g for the TM_1 magnetic resonance. Clearly, the strong magnetic and electric dipole–dipole coupling for Au results in a marked dependence of the cross section per SRR on array lattice constant. For the ITO SRRs, the dependence on interparticle coupling is virtually absent. Overall, the cross section of the ITO SRRs is reduced compared to Au, which can be attributed to the low electron density and resulting polarizability.[39] The experimental results are in good agreement with the cross sections obtained from simulations (lines) for both the Au and ITO metamaterials. Supporting Information, Figure S4, shows the behavior for the TE_1 resonance for the ITO SRRs. The corresponding mode in Au is strongly affected by the interparticle coupling and is shifted out of the experimentally accessible range of the FTIR spectrometer for high densities. The TE response confirms the general picture of weakly interacting SRRs for the case of ITO.

The finite permittivity of ITO allow achieving extremely dense metamaterials. Up to 80 elements per square wavelength are achieved at the TM_1 resonance wavelength of 6 μm (50 THz) and for an array period a = 700 nm. In comparison, the equivalent metamaterial made from Au has a fundamental TM_1 resonance at around 2 μm (150 THz) and thus a density of only eight elements per square wavelength.

The dielectric properties of ITO can be tuned through the carrier concentration. In order to investigate the effect of carrier density on the magnetic and electric resonances of the SRRs, we performed simulations using a Drude model for the dielectric function of the ITO, given by

$$\varepsilon = \varepsilon_\infty - \frac{{\omega_{pl}}^2}{\omega^2 - i\omega\Gamma} \quad (1)$$

where the plasma frequency is given by $\omega_{pl} = (Ne^2/(\varepsilon_0 m^*))^{1/2}$, with N the carrier concentration and m^* the effective mass, which is 0.4× the electron rest mass. The dielectric background permittivity is given by ε_∞ = 3.8, while the relaxation energy Γ = 0.13 eV arises from a 5 fs plasmon dephasing time.[23,36,40] Simulations of SRR arrays were undertaken, using the same geometry as the experimental design parameters, w = 400 nm and a = 850 nm. Periodic boundary conditions were used to create an infinite 2-D metamaterial. Figure 4a,b shows the simulated transmission for carrier densities ranging from 10^{20} cm^{-3} to 10^{22} cm^{-3}, for TM (a) and TE (b) polarizations, corresponding reflection maps are shown in Supporting Information, Figure S5a,b. Both the lower order TM modes and the TE modes can be recognized by the dips in transmission and show a pronounced wavelength scaling as a function of carrier density. The low electron density results in a reduced screening and hence increased penetration depth of fields in the dielectric. Thus, compared to a perfect metal, the electromagnetic modes are more susceptible to the permittivity of the plasmonic metal and as a consequence the surface plasmon wavelength is reduced. As a consequence, the

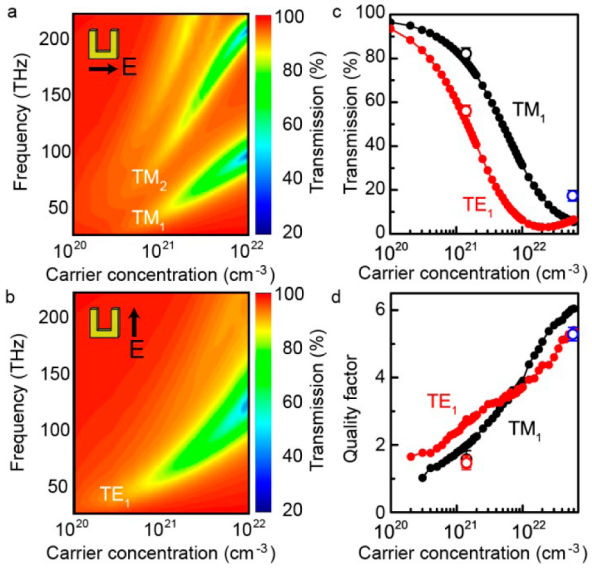

Figure 4. (a, b) Simulated transmission through SRR metamaterials made from a ITO-like Drude metal of varying carrier density between 10^{20}–10^{22} cm^{-3}, for horizontal (TM) and vertical (TE) polarizations. (c, d) Transmission (c) and quality factor (d) of TM_1 and TE_1 modes vs carrier concentration. Closed symbols, simulations; open symbols, experimental results for ITO (black TM_1, red TE_1) and Au (blue, TM_1).

DOI: 10.1021/acsphotonics.5b00089
ACS Photonics 2015, 2, 606–614

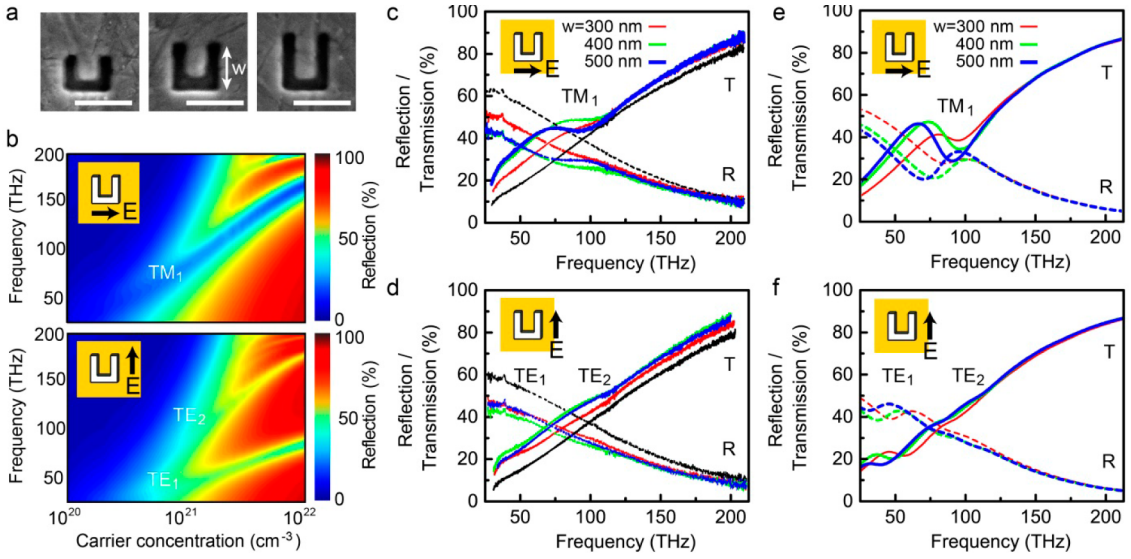

Figure 5. (a) SEM images of c-SRRs produced by FIB milling into an ITO film, corresponding to arm length w = 300 (left), 400 (middle), and 500 nm (right). Scale bars, 500 nm. (b) Simulated spectral maps for reflection from a w = 400 nm c-SRR array, using an ITO-like Drude metal of varying carrier density between 10^{20}–10^{22} cm^{-3}, for horizontal (TM) and vertical (TE) polarization. (c, d) Experimental transmission and reflection spectra for ITO c-SRR metamaterials for horizontal (c, TM) and vertical (d, TE) polarizations, black lines: ITO substrate. (e, f) Numerical model simulations of corresponding metamaterial arrays of c and d, for free carrier density of 7×10^{20} cm^{-3}.

resonances shift to lower frequency for reduced electron densities. This trend demonstrated the wide tunability of ITO metamaterial resonances by varying the carrier density, either at fabrication or through electrical or optical control.

For electron densities around 10^{20} cm^{-3}, the ITO material loses its metallic properties, which can be observed as a gradual disappearance of the resonant modes of the SRR. To further analyze this trend, we extracted the amplitude and quality factor of the transmission dip at resonance for the TM_1 and TE_1 modes, as is shown in Figure 4c,d. We see that the amplitude of the magnetic mode is more sensitive to the carrier density than the electric mode. Clearly the electric dipole strength is higher and saturates at lower carrier densities than the induced magnetic moment. The quality factors, shown in Figure 4d, show a similar trend, namely, a steeper reduction of the quality factor of the TM_1 mode than the TE_1 mode, indicating that the electric resonance can be sustained at lower carrier densities than the magnetic mode. The quality factors of the two modes cross around 10^{22} cm^{-3} as the TM_1 mode becomes more prominent, while the TE_1 resonance reaches saturation. The experimentally observed resonance strength and quality factor for ITO and Au are indicated by the open symbols in Figure 4c,d. Reasonable agreement is obtained with the simulated behavior, demonstrating that the main differences between the Au and ITO metamaterial response can be attributed primarily to the difference in carrier density.

ITO Complementary Metamaterial Arrays. Next to direct designs, we experimentally investigate ITO complementary SRR (c-SRR) metamaterial arrays obtained by focused ion beam milling (FIB). As a consequence of Babinet's principle, an SRR etched into an infinite, perfectly conducting film is expected have a resonance at the same frequency position as the SRR on its own, although for the opposite polarization. Babinet/complementary metamaterials consisting of c-SRRs have been investigated in the literature, as has the general applicability of Babinet's principle to composite metamaterials.[57,58] In the case of ITO, the approximations underpinning Babinet's principle are less robust since ITO is less metallic than noble metals, so we aim to find if the Babinet's principle approach remains useful when dealing with ITO, and to investigate the characteristics of complementary ITO metamaterials.

Figure 5a shows SEM images of the c-SRR arrays fabricated using FIB with a fixed width of 400 nm and varying arm lengths w of 300, 400, and 500 nm. For the c-SRR metamaterial, numerical simulations predict the appearance of spectral modes similar to the direct SRRs, but for opposite polarizations. Figure 5b shows the calculated reflection from the 80 nm thick c-SRR array corresponding to the fabricated structure, as a function of carrier concentration. The scaling of the lowest order modes TE_1 and TE_2 compares well with the TM modes of Figure 4a, while the c-SRR TM_1 mode follows the TE_1 mode of the direct metamaterial. The modes in Figure 5b appear as dips in the reflectivity, which is expected from Babinet's principle, which states that the roles of reflection and transmission are reversed. Corresponding transmission maps for the c-SRR are shown in Supporting Information, Figure S5c,d. The breakdown of the metallic regime is observed below 10^{21} cm^{-3} as a reduction of the reflectivity and concomitant suppression of the c-SRR resonances.

It was found that the conditions in FIB processing resulted in a strong reduction of the carrier concentration of the entire ITO sample. An additional 2 h annealing step after FIB was necessary to increase the carrier density to a level comparable to that of the initial film. Supporting Information, Figure S6, shows the effect of this annealing on the optical response. While good results were obtained by the annealing, the recovered carrier density of 7×10^{20} cm^{-3} was around a factor two lower than that of the film before FIB milling. The experimentally obtained response of the c-SRR arrays after annealing is presented in Figure 5c and d for TM and TE polarizations, respectively. Evidence of the resonant response is most clearly observed in the spectra for TM polarization, which reveals the presence of the TM_1 electric mode. The shift of the resonances with different structures confirms the direct relation of the mode with the metamaterial geometry, in agreement with

DOI: 10.1021/acsphotonics.5b00089
ACS Photonics 2015, 2, 606–614

numerical simulations presented in Figure 5e,f. For TE polarization only very weakly resonant behavior was found in transmission, and no clear resonances in reflection, in qualitative agreement with numerical simulations which also show much less pronounced magnetic resonances. Reasonably good agreement between experimental and simulated spectra was obtained for a carrier density of 7×10^{20} cm^{-3}, especially for TM polarization, whereas the simulated TE spectra predicts features which were not pronounced enough to be resolved in experimental data. The resonances appear as dispersive line shapes due to (Fano-type) interference of the resonant metamaterial features with the nonresonant background.

Compared to the direct SRRs, the c-SRRs show a strongly reduced performance in the strength of the metamaterial response, both in simulation and in experiment. The origin of this difference can be identified by comparing the distribution of electromagnetic fields in both geometries. Figure 6 shows the

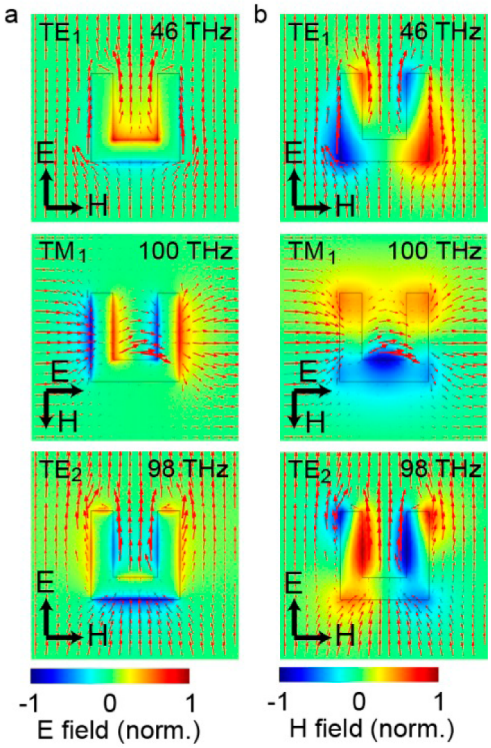

Figure 6. (a, b) Maps showing out of plane E-field (a) and H-field (b) for the first three resonant modes of the ITO inverse SRRs, together with vector fields (red arrows) representing current density.

near field maps of the perpendicular field components and current density for the c-SRR. For the direct SRR, Figure 2e,f shows that resonant fields are largest outside of the ITO structure. The situation is reversed for the c-SRR in Figure 6a,b, where the fields and currents are seen to strongly penetrate into the ITO film where they are more susceptible to losses. Thus, the finite penetration depth of fields, which is responsible for the strongly reduced resonator size, results in the c-SRR geometry to be much less favorable for low permittivity materials such as metal oxides.

Figure 6 also shows the complementary principle where not only the TM and TE modes are reversed, but also the symmetry of the E- and H-fields. Thus, the numerical simulations demonstrate that Babinet's principle holds qualitatively for the case of ITO metamaterials and their complementary structures, even at moderate carrier densities.

DISCUSSION

The above results on direct and complementary metamaterials clearly point out the opportunities and limitations offered by metal oxides for applications. Clearly, metal oxide plasmonics and metamaterials do not compete with noble metals in terms of quality of the resonant response but rather are driven by a range of practical applications where complementary properties such as tunability, transparency in the optical range and chemical or electrical activity could be combined with resonant infrared response. Our results show the possible performance that can be achieved using carrier densities of around 10^{21} cm^{-3}, which are the highest carrier densities possible for these type of materials. Light−matter interactions are significantly reduced compared to high-density noble metals, however still resonant response of up to 50% in transmission can be achieved exploiting the compact resonator size and very high packing density achievable using metal oxides. The resulting structures are sufficient for a range of applications where 100% interaction is not required, including sensing or coherent absorption devices.[59] The overall interaction strength may be further improved by changing the design, for example using 3D stacking of metamaterials or by employing reflectarrays.

Gradient metasurfaces will benefit from homogeneous phase gradients and the ability to produce extremely steep gradients offered by high-density ITO metasurfaces. The ratio of the highest in-plane spatial frequency $k_{||} = \pi/a$ to the incident wavevector k_0 is a measure of the precision with which an incident wavefront can be constructed. For the ITO metamolecules of our study, the ratio $k_{||}/k_0$ reaches up to 4.2, while for Au the highest value lies around 1.4. Thus, ITO metasurfaces may allow more accurate wavefront synthesis with less discretization artifacts, or multiplexing of different functionalities (i.e., wavelengths, polarization) into one metasurface. Additionally, ITO metasurfaces can be designed to provide very high spatial frequency components, which is of interest for example for coupling light into high-index substrates and solid-immersion metalenses. In contrast to conventional noble-metal resonators, ITO-based metasurfaces provide subdiffraction performance up to the fourth harmonic, which makes them extremely interesting for nonlinear metasurfaces where both the fundamental and harmonic frequencies require a homogeneous metamaterial response.

The low permittivity of metal oxides results in significant penetration of fields inside the material. On the one hand this penetration results in a strongly reduced plasmon wavelength and a concomitantly smaller size of the resonator, which is of interest for applications requiring a homogeneous metamaterial response. On the other hand, field penetration results in more lossy resonances, in particular, for the complementary structures. Our results show that direct structures, where the volume of metal oxide material is relatively small, offer a feasible platform for oxide plasmonics, whereas complementary structures are generally too lossy to sustain the metamaterial resonances. While losses are generally unfavorable, the resulting broad resonances can offer a large bandwidth of operation of interest for example for infrared spectroscopy, broadband filters, and energy harvesting.

DOI: 10.1021/acsphotonics.5b00089
ACS Photonics 2015, 2, 606−614

CONCLUSIONS

In conclusion, we have fabricated split-ring metamaterials using the transparent conductive oxide ITO as the plasmonic material. We have shown that the resonances of these metamaterials are red-shifted and less pronounced compared to corresponding Au metamaterial arrays. The reduced strength and higher losses make ITO metamaterials less favorable as a material for plasmonics than conventional noble metals, however the increased bandwidth and optical transparency will be of interest for a range of applications. In particular, the constituent metamolecules, when built from ITO, may be packed much more densely without the influence of interparticle interactions. This could be used to create much more subwavelength metamaterials or gradient metasurfaces with concomitantly improved homogenization of optical response. We demonstrated a resonant response of up to 50% in transmission, which, in conjunction with properties such as tunability, compatibility with silicon processing, and chemical activity, make TCOs an attractive alternative plasmonic material in the near- and mid-infrared. Additionally, we have explored through simulations the tuning of ITO metamaterials through material parameters by varying the carrier concentration of the ITO. A lower carrier concentration decreases the resonant frequencies of a metamaterial but at a cost to the quality of the resonances. By milling of complementary metamaterials into an ITO film, we found that Babinet's principle may be applied to obtain a qualitative description of metamaterial resonances in the regime where losses are sufficiently weak.

EXPERIMENTAL SECTION

ITO Deposition. ITO films were deposited by e-beam evaporation (ITO grains, 90−10 wt % 99.99 pure from Testbourne Ltd., U.K.) on a calcium fluoride (CaF_2) substrate in 2×10^{-4} mbar partial oxygen pressure, after achieving a base pressure of 2×10^{-6} mbar. The films were subsequently annealed at 200 °C for 1 h. Hall measurement revealed a carrier density of 5×10^{20} cm^{-3}, while ellipsometry data could be fitted by a Drude model with a free carrier density of 1.25×10^{21} cm^{-3}.

Metamaterial Fabrication. Metamaterial arrays were fabricated by e-beam lithography (JEOL 9300FS) using a 3-layer lift-off technique. A 150 PMMA layer was spin coated, followed by a sputtered 20 nm SiO_2 layer and a spin coated MMA layer of 50 nm thickness. Following e-beam lithography, the top MMA layer was developed and used as a mask for dry-etching of the SiO_2. The final wet etching step produced gaps with a strongly reduced undercut compared to conventional two-layer resists, which allowed achieving extremely high densities of metamolecules. For comparison Au metamaterial arrays with identical design parameters were fabricated. Inverse metamaterials were milled into a continuous ITO film using focused ion beam (FIB) milling using a FEI Helios Nanolab 600.

Infrared Spectroscopy. Infrared spectra were measured in transmission and reflection using a Jasco FTIR-4200 with a liquid-nitrogen-cooled mercury cadmium telluride detector. A blank CaF_2 substrate was used as a reference for transmission, while a silver mirror was used as reference for reflection. Spectra were taken for both horizontal and vertical polarized light to investigate the magnetic and electric modes of the SRR arrays, respectively. Measurements were taken with a resolution of 4 cm^{-1}.

Numerical Simulations. Finite element simulations were performed using COMSOL Multiphysics, using periodic boundary conditions for the simulation walls and scattering boundary conditions for the simulation entrance/exit. SRRs of identical geometry to the design parameters were modeled with a Drude model used for ITO and Sellmeier model for CaF_2. Simulations used a linear iterative solver with a relative tolerance of 0.001. Minimum mesh element quality was 0.1328 for complementary metamaterials and 0.2101 for direct metamaterials.

ASSOCIATED CONTENT

Supporting Information

Additional experiments on polarization dependence, dependence on array period for TE polarization, and effect of annealing for complementary SRRs. Additional simulations of dependence of resonances on metamaterial geometry and carrier density. The Supporting Information is available free of charge on the ACS Publications website at DOI: 10.1021/acsphotonics.5b00089.

AUTHOR INFORMATION

Corresponding Author

*E-mail: o.muskens@soton.ac.uk.

Notes

The authors declare no competing financial interest.

ACKNOWLEDGMENTS

The authors thank N. Zheludev for stimulating discussions and O. Buchnev for technical support with the focused ion beam. SG acknowledges financial support by Dstl through a UK Ph.D. studentship. This work was financially supported by EPSRC through research grant EP/J011797/1 and through the Nanostructured Photonic Metamaterials Programme EP/G060363/1. O.M. acknowledges support through EPSRC Fellowship EP/J016918/1. The data for this paper can be found at 10.5258/SOTON/376381.

REFERENCES

(1) Soukoulis, C. M.; Wegener, M. Past Achievements and Future Challenges in the Development of Three-Dimensional Photonic Metamaterials. *Nat. Photonics* **2011**, *5*, 523−530.
(2) Zheludev, N. I.; Kivshar, Y. S. From Metamaterials to Metadevices. *Nat. Mater.* **2012**, *11*, 917−924.
(3) Landy, N.; Smith, D. R. A Full-Parameter Unidirectional Metamaterial Cloak for Microwaves. *Nat. Mater.* **2012**, *12*, 25−28.
(4) Ergin, T.; Stenger, N.; Brenner, P.; Pendry, J. B.; Wegener, M. Three-Dimensional Invisibility Cloak at Optical Wavelengths. *Science* **2010**, *328*, 337−339.
(5) Pendry, J. Negative Refraction Makes a Perfect Lens. *Phys. Rev. Lett.* **2000**, *85*, 3966−3969.
(6) Fang, N.; Lee, H.; Sun, C.; Zhang, X. Sub-Diffraction-Limited Optical Imaging with a Silver Superlens. *Science* **2005**, *308*, 534−537.
(7) Landy, N.; Sajuyigbe, S.; Mock, J.; Smith, D.; Padilla, W. Perfect Metamaterial Absorber. *Phys. Rev. Lett.* **2008**, *100*, 207402.
(8) Liu, N.; Mesch, M.; Weiss, T.; Hentschel, M.; Giessen, H. Infrared Perfect Absorber and Its Application as Plasmonic Sensor. *Nano Lett.* **2010**, *10*, 2342−2348.
(9) Yu, N.; Capasso, F. Flat Optics with Designer Metasurfaces. *Nat. Mater.* **2014**, *13*, 139−150.

DOI: 10.1021/acsphotonics.5b00089
ACS Photonics 2015, 2, 606−614

(10) Li, X.; Xiao, S.; Cai, B.; He, Q.; Cui, T. J.; Zhou, L. Flat Metasurfaces to Focus Electromagnetic Waves in Reflection Geometry. *Opt. Lett.* **2012**, *37*, 4940−4942.
(11) Larouche, S.; Tsai, Y.-J.; Tyler, T.; Jokerst, N. M.; Smith, D. R. Infrared Metamaterial Phase Holograms. *Nat. Mater.* **2012**, *11*, 450−454.
(12) Huang, L.; Chen, X.; Mühlenbernd, H.; Zhang, H.; Chen, S.; Bai, B.; Tan, Q.; Jin, G.; Cheah, K.-W.; Qiu, C.-W.; Li, J.; Zentgraf, T.; Zhang, S. Three-Dimensional Optical Holography Using a Plasmonic Metasurface. *Nat. Commun.* **2013**, *4*, 2808.
(13) Cao, L.; Fan, P.; Barnard, E. S.; Brown, A. M.; Brongersma, M. L. Tuning the Color of Silicon Nanostructures. *Nano Lett.* **2010**, *10*, 2649−2654.
(14) Zhou, J.; Chowdhury, D. R.; Zhao, R.; Azad, A. K.; Chen, H.-T.; Soukoulis, C. M.; Taylor, A. J.; O'Hara, J. F. Terahertz Chiral Metamaterials with Giant and Dynamically Tunable Optical Activity. *Phys. Rev. B* **2012**, *86*, 035448.
(15) Fan, K.; Hwang, H. Y.; Liu, M.; Strikwerda, A. C.; Sternbach, A.; Zhang, J.; Zhao, X.; Zhang, X.; Nelson, K. a.; Averitt, R. D. Nonlinear Terahertz Metamaterials via Field-Enhanced Carrier Dynamics in GaAs. *Phys. Rev. Lett.* **2013**, *110*, 217404.
(16) Belotelov, V. I.; Kreilkamp, L. E.; Akimov, I. A.; Kalish, A. N.; Bykov, D. A.; Kasture, S.; Yallapragada, V. J.; Venu Gopal, A.; Grishin, a M.; Khartsev, S. I.; Nur-E-Alam, M.; Vasiliev, M.; Doskolovich, L. L.; Yakovlev, D. R.; Alameh, K.; Zvezdin, A. K.; Bayer, M. Plasmon-Mediated Magneto-Optical Transparency. *Nat. Commun.* **2013**, *4*, 2128.
(17) Ou, J.-Y.; Plum, E.; Zhang, J.; Zheludev, N. I. An Electromechanically Reconfigurable Plasmonic Metamaterial Operating in the near-Infrared. *Nat. Nanotechnol.* **2013**, *8*, 252−255.
(18) Papasimakis, N.; Thongrattanasiri, S.; Zheludev, N. I.; García de Abajo, F. The Magnetic Response of Graphene Split-Ring Metamaterials. *Light Sci. Appl.* **2013**, *2*, e78.
(19) Staude, I.; Decker, M.; Rusak, E.; Neshev, D. N.; Brener, I. Active Tuning of All-Dielectric Metasurfaces. *ACS Nano* **2015**, DOI: 10.1021/acsnano.5b00723.
(20) Yang, Y.; Wang, W.; Moitra, P.; Kravchenko, I. I.; Briggs, D. P.; Valentine, J. Dielectric Meta-Reflectarray for Broadband Linear Polarization Conversion and Optical Vortex Generation. *Nano Lett.* **2014**, *14*, 1394−1399.
(21) Wu, C.; Arju, N.; Kelp, G.; Fan, J. A.; Dominguez, J.; Gonzales, E.; Tutuc, E.; Brener, I.; Shvets, G. Spectrally Selective Chiral Silicon Metasurfaces Based on Infrared Fano Resonances. *Nat. Commun.* **2014**, *5*, 3892.
(22) Decker, M.; Staude, I.; Falkner, M.; Dominguez, J.; Neshev, D. N.; Brener, I.; Pertsch, T.; Kivshar, Y. S. High-Efficiency Dielectric Huygen's Surface. *Adv. Opt. Mater.* **2015**, DOI: 10.1002/adom.201400584.
(23) Kim, J.; Naik, G. V.; Emani, N. K.; Guler, U.; Boltasseva, A. Plasmonic Resonances in Nanostructured Transparent Conducting Oxide Films. *IEEE J. Sel. Top. Quantum Electron.* **2013**, *19*, 4601907−4601907.
(24) Naik, G. V.; Liu, J.; Kildishev, A. V.; Shalaev, V. M.; Boltasseva, A. Demonstration of Al:ZnO as a Plasmonic Component for near-Infrared Metamaterials. *Proc. Natl. Acad. Sci. U.S.A.* **2012**, *109*, 8834−8838.
(25) Tassin, P.; Koschny, T.; Kafesaki, M.; Soukoulis, C. M. A Comparison of Graphene, Superconductors and Metals as Conductors for Metamaterials and Plasmonics. *Nat. Photonics* **2012**, *6*, 259−264.
(26) Bobb, D. A.; Zhu, G.; Mayy, M.; Gavrilenko, A. V.; Mead, P.; Gavrilenko, V. I.; Noginov, M. A. Engineering of Low-Loss Metal for Nanoplasmonic and Metamaterials Applications. *Appl. Phys. Lett.* **2009**, *95*, 151102.
(27) Naik, G. V.; Schroeder, J. L.; Ni, X.; Kildishev, A. V.; Sands, T. D.; Boltasseva, A. Titanium Nitride as a Plasmonic Material for Visible and near-Infrared Wavelengths. *Opt. Mater. Express* **2012**, *2*, 478.
(28) Gu, L.; Livenere, J.; Zhu, G.; Narimanov, E. E.; Noginov, M. A. Quest for Organic Plasmonics. *Appl. Phys. Lett.* **2013**, *103*, 021104.
(29) Yan, H.; Li, X.; Chandra, B.; Tulevski, G.; Wu, Y.; Freitag, M.; Zhu, W.; Avouris, P.; Xia, F. Tunable Infrared Plasmonic Devices Using Graphene/Insulator Stacks. *Nat. Nanotechnol.* **2012**, *7*, 330−334.
(30) Ou, J.-Y.; So, J.-K.; Adamo, G.; Sulaev, A.; Wang, L.; Zheludev, N. I. Ultraviolet and Visible Range Plasmonics in the Topological Insulator $Bi_{1.5}Sb_{0.5}Te_{1.8}Se_{1.2}$. *Nat. Commun.* **2014**, *5*, 1−7.
(31) Kinsey, N.; Ferrera, M.; Shalaev, V. M.; Boltasseva, A. Examining Nanophotonics for Integrated Hybrid Systems: A Review of Plasmonic Interconnects and Modulators Using Traditional and Alternative Materials [Invited]. *J. Opt. Soc. Am. B* **2014**, *32*.
(32) Ginn, J.; Shelton, D.; Krenz, P.; Lail, B.; Boreman, G. Altering Infrared Metamaterial Performance through Metal Resonance Damping. *J. Appl. Phys.* **2009**, 105.
(33) Khurgin, J. B. How to Deal with the Loss in Plasmonics and Metamaterials. *Nat. Nanotechnol.* **2015**, *10*, 2−6.
(34) Lee, H. W.; Papadakis, G.; Burgos, S. P.; Chandler, K.; Kriesch, A.; Pala, R.; Peschel, U.; Atwater, H. A. Nanoscale Conducting Oxide PlasMOStor. *Nano Lett.* **2014**, *14*, 6463−6468.
(35) Feigenbaum, E.; Diest, K.; Atwater, H. A. Unity-Order Index Change in Transparent Conducting Oxides at Visible Frequencies. *Nano Lett.* **2010**, *10*, 2111−2116.
(36) Naik, G. V.; Shalaev, V. M.; Boltasseva, A. Alternative Plasmonic Materials: Beyond Gold and Silver. *Adv. Mater.* **2013**, *25*, 3264−3294.
(37) Guler, U.; Boltasseva, A.; Shalaev, V. M. Refractory Plasmonics. *Science* **2014**, *344*, 263−264.
(38) Kim, H.; Gilmore, C. M.; Piqué, A.; Horwitz, J. S.; Mattoussi, H.; Murata, H.; Kafafi, Z. H.; Chrisey, D. B. Electrical, Optical, and Structural Properties of Indium−Tin−Oxide Thin Films for Organic Light-Emitting Devices. *J. Appl. Phys.* **1999**, *86*, 6451.
(39) Abb, M.; Wang, Y.; Papasimakis, N.; de Groot, C. H.; Muskens, O. L. Surface-Enhanced Infrared Spectroscopy Using Metal Oxide Plasmonic Antenna Arrays. *Nano Lett.* **2014**, *14*, 346−352.
(40) Rhodes, C.; Franzen, S.; Maria, J.-P.; Losego, M.; Leonard, D. N.; Laughlin, B.; Duscher, G.; Weibel, S. Surface Plasmon Resonance in Conducting Metal Oxides. *J. Appl. Phys.* **2006**, *100*, 054905.
(41) Noginov, M. A.; Gu, L.; Livenere, J.; Zhu, G.; Pradhan, A. K.; Mundle, R.; Bahoura, M.; Barnakov, Y. A.; Podolskiy, V. A. Transparent Conductive Oxides: Plasmonic Materials for Telecom Wavelengths. *Appl. Phys. Lett.* **2011**, *99*, 021101.
(42) Li, S.; Guo, P.; Zhang, L.; Zhou, W. Infrared Plasmonics with Indium−Tin-Oxide Nanorod Arrays. *ACS Nano* **2011**, *5*, 9161−9170.
(43) Ellmer, K. Past Achievements and Future Challenges in the Development of Optically Transparent Electrodes. *Nat. Photonics* **2012**, *6*, 809−817.
(44) Gershon, T. Metal Oxide Applications in Organic-Based Photovoltaics. *Mater. Sci. Technol.* **2011**, *27*, 1357−1371.
(45) Fortunato, E.; Ginley, D.; Hosono, H.; Paine, D. C. Transparent Conducting Oxides for Photovoltaics. *MRS Bull.* **2007**, *32*, 242−247.
(46) Zhang, X.; Chen, Y. L.; Liu, R.-S.; Tsai, D. P. Plasmonic Photocatalysis. *Rep. Prog. Phys.* **2013**, *76*, 046401.
(47) Camagni, P.; Faglia, G.; Galinetto, P. Photosensitivity Activation of SnO_2 Thin Film Gas Sensors at Room Temperature. *Sens. Actuators, B* **1996**, *31*, 99−103.
(48) Miyata, T.; Hikosaka, T.; Minami, T. High Sensitivity Chlorine Gas Sensors Using Multicomponent Transparent Conducting Oxide Thin Films. *Sens. Actuators, B* **2000**, *69*, 16−21.
(49) Sorger, V. J.; Lanzillotti-Kimura, N. D.; Ma, R.-M.; Zhang, X. Ultra-Compact Silicon Nanophotonic Modulator with Broadband Response. *Nanophotonics* **2012**, *1*, 17−22.
(50) Abb, M.; Wang, Y.; de Groot, C. H.; Muskens, O. L. Hotspot-Mediated Ultrafast Nonlinear Control of Multifrequency Plasmonic Nanoantennas. *Nat. Commun.* **2014**, *5*, 4869.
(51) Caglayan, H.; Hong, S.-H.; Edwards, B.; Kagan, C. R.; Engheta, N. Near-Infrared Metatronic Nanocircuits by Design. *Phys. Rev. Lett.* **2013**, *111*, 073904.
(52) Traviss, D.; Bruck, R.; Mills, B.; Abb, M.; Muskens, O. L. Ultrafast Plasmonics Using Transparent Conductive Oxide Hybrids in the Epsilon-near-Zero Regime. *Appl. Phys. Lett.* **2013**, *102*, 121112.

DOI: 10.1021/acsphotonics.5b00089
ACS Photonics 2015, 2, 606−614

(53) Tsakmakidis, K. L.; Pickering, T. W.; Hamm, J. M.; Page, A. F.; Hess, O. Completely Stopped and Dispersionless Light in Plasmonic Waveguides. *Phys. Rev. Lett.* **2014**, *112*, 167401.
(54) Liu, J.; Naik, G. V.; Ishii, S.; Devault, C.; Boltasseva, A.; Shalaev, V. M.; Narimanov, E. Optical Absorption of Hyperbolic Metamaterial with Stochastic Surfaces. *Opt. Express* **2014**, *22*, 8893−8901.
(55) Zhou, J.; Koschny, T.; Soukoulis, C. M. Magnetic and Electric Excitations in Split Ring Resonators. *Opt. Express* **2007**, *15*, 17881−17890.
(56) Sersic, I.; Frimmer, M.; Verhagen, E.; Koenderink, A. F. Electric and Magnetic Dipole Coupling in Near-Infrared Split-Ring Metamaterial Arrays. *Phys. Rev. Lett.* **2009**, *103*, 213902.
(57) Rockstuhl, C.; Zentgraf, T.; Meyrath, T. P.; Giessen, H.; Lederer, F. Resonances in Complementary Metamaterials and Nanoapertures. *Opt. Express* **2008**, *16*, 2080−2090.
(58) Zentgraf, T.; Meyrath, T.; Seidel, A.; Kaiser, S.; Giessen, H.; Rockstuhl, C.; Lederer, F. Babinet's Principle for Optical Frequency Metamaterials and Nanoantennas. *Phys. Rev. B* **2007**, *76*, 033407.
(59) Zhang, J.; MacDonald, K. F.; Zheludev, N. I. Controlling Light-with-Light without Nonlinearity. *Light Sci. Appl.* **2012**, *1*, e18.

DOI: 10.1021/acsphotonics.5b00089
ACS Photonics 2015, 2, 606−614